The effects of plasticizer agent in mesoporous phosphotungstic acid modified chitosan membrane and its performances for direct methanol fuel cell application

Lukman Atmaja[a], **Arif Priyangga**[a,*], **Yohana Ivana Kedang**[a,b], **Mardi Santoso**[a], **Juhana Jaafar**[c], **Djoko Hartanto**[a]

[a] Department of Chemistry, Faculty of Science and Data Analytics, Institut Teknologi Sepuluh Nopember, Surabaya 60111 Indonesia
[b] Department of Chemistry, Faculty of Agriculture, Universitas Timor, Kefamenanu 85613 Indonesia
[c] Advanced Membrane Technology (AMTEC) Research Centre, Universiti Teknologi Malaysia, UTM Johor Bahru, Johor 81310 Malaysia

*Corresponding author, e-mail: arifpriyangga97@gmail.com

ABSTRACT: Chitosan (Cs) is an attractive material with outstanding properties such as excellent film-forming properties, biodegradability, and ease of chemical modification. The Cs membrane is usually applied as part of the proton exchange membrane (PEM) material in fuel cell applications. The drawbacks of the Cs membrane can be surmounted by applying the hydrophilic/plasticizer agent and combining the modified heteropoly acid filler. In this research, the Cs membrane was successfully fabricated using a solvent-evaporation method with the incorporation of mesoporous phosphotungstic acid (m-PTA) and glycerol (gly). The outstanding performances were obtained by the Cs/gly-1/m-PTA membrane, which had the first degradation temperature up to 200 °C, chemical stability with the lowest weight loss at 18.33±0.762%, and the highest proton conductivity at 5.13 mS/cm. The other performances exchange capacity (IEC) at 2.949±0.022 mmol/g, and water and methanol uptake at 89.05±0.092% and 1.26±0.031%, respectively. In comparison to the pristine Cs membrane, which exhibits lower proton conductivity and higher methanol permeability at 2.40 mS/cm and 1.003×10^{-5} cm^2/s, respectively, the addition of m-PTA filler and gly as a plasticizer agent increases the performance of the chitosan properties used in direct methanol fuel cell membranes.

KEYWORDS: chitosan, mesoporous phosphotungstic acid, glycerol, proton exchange membrane, direct methanol fuel cell

INTRODUCTION

A fuel cell is an alternative piece of equipment that converts chemical energy to electricity through a redox reaction and has excellent conversion efficiency as long as the fuel is supplied [1]. Direct methanol fuel cell (DMFC) is one of the fuel cell types with water and methanol as fuels. The advantages of DMFC usage are easy operation and storage, low emission, high energy density, and low cost of fuel [2]. Although the DMFC operates at low operating temperatures up to 80 °C, some challenges should be tackled such as the proton exchange membrane (PEM), catalyst, anode, and cathode. PEM is one of the important components in fuel cells that provide proton pathways [3]. The challenges of PEM itself include thermal and chemical stability, methanol permeability, proton transfer in the membrane, and water retention capability [4]. Outstanding water retention can manage the proton transport of the membrane, increasing its conductivity [5]. Moreover, the high methanol crossover is not favorable in fuel cells due to low fuel efficiency. High proton conductivity and low methanol permeability are some parameters that need to be fulfilled for developing a novel composite membrane [6].

Nafion is the commercial membrane for a fuel cell that is commonly used as a PEM for DMFC. Although Nafion also suffers high methanol crossover during the long-term and high-temperature operation of fuel cells [7] at room temperature, Nafion has a methanol permeability of 1.44×10^{-6} cm^2/s and 7.92×10^{-6} cm^{2}s at 70 °C. The increasing value of its permeability also affects the membrane selectivity [8]. The properties of its materials, including the polymer, considerably prevent the excess of methanol crossover [9]. Alternative polymer materials have been developed, including cellulose, carrageenan, and chitosan. Those polymers are classified as biopolymers that have biocompatibility, low-cost material, and high water retention due to their hydrophilicity [10].

Chitosan (Cs) is the most abundant biopolymer after cellulose which is isolated from the Crustaceans with a degree of deacetylation ⩾75% [7]. Cs is desirable as an alternative PEM due to its compatibility, biodegradability, less toxicity, ease of modification, and good film-forming properties [9]. High methanol permeability is also achieved by pristine Cs membrane, which decreases their efficiency. The permeability of a pristine Cs membrane is 4.24×10^{-6} cm^2/s with low thermal stability [10]. However, the addition of inorganic filler such as polyoxometalate material can

diminish the permeability, as reported in the previous study that the addition of phosphotungstic acid (PTA) into nanocrystalline cellulose (NCC) membrane can diminish its permeability to 8.28×10^{-7} cm^2/s and boost its conductivity to 13.17 mS/cm [7]. Due to the leaching process during the operation, PTA was modified to mesoporous PTA without decreasing its performance. The thermal stability was obtained until 450 °C, and it was applied to a lithium-ion battery that obtained the capacity of 872 mAh/g for 100 cycles [11]. PTA chemically acts as a donor proton and is classified as a strong Bronsted acid, which is very useful to improve the proton transfer in PEM [12]. Furthermore, the plasticizer agent can be a solution to improve the interaction between polymer and inorganic filler. More interactions involved in the membrane structure make the membrane more homogeneous and cause less agglomeration [13]. The enhancement of water absorption was also shown in the previous study that the addition of glycerol (gly) into sodium alginate/sulfonated graphene oxide can increase its water uptake to 137% with a power density of 13.6 mW/cm^2 [4]. Another study was also conducted utilizing the Cs/Alginate (Alg) membrane with various plasticizer agents, including phosphoric acid, sulfuric acid, and glycerol. The result showed the enhancement of its performances and properties, such as the Cs/Alg membrane without the plasticizer agent, and the increase of its power density from 237 mW/m^3 to 365 mW/m^3. The addition of phosphoric and sulfuric acids increased the tensile strength to 7.7 and 7.6 N/mm^2, respectively. It also showed that gly exhibited the most flexibility with 6.8 N/mm^2 and 8.9% for its tensile strength and elongation, respectively. The decreasing intermolecular attraction and increasing polymer mobility led the film to be more flexible [14]. The composite Cs:NH$_4$I:Zn(II)-complex membrane showed improved ionic conductivity and dielectric properties with increasing gly concentration. The composition of 30 wt.% gly exhibited the highest dielectric constant with an optimum ionic conductivity of 1.17×10^{-4} S/cm [15]. Gly is the common plasticizer for biopolymers including Cs. The presence of gly in the Cs membrane prepared via a heat-mechanical treatment method increased the water uptake and elongation at a break, which reached 40% [16].

High surface area and sulfonate groups support proton transfer in the membranes, as mentioned in several previous studies that they had higher proton conductivity than commercial Nafion. The SPEEK/-MOF membrane had an optimum conductivity of 104 mS/cm at room temperature operation [17], the SPEEK/sSrZrO$_3$@TiO$_2$ membrane had an ionic conductivity of 120.9 mS/cm at 80 °C [18], and the SPEEK/sBH/SnO$_2$ membrane had a conductivity of 92.01 mS/cm at 80 °C [19]. Based on the short review, this research is to present a study of a novel Cs/m-PTA

membrane with the addition of gly as a plasticizer to improve the membrane properties, including its proton conductivity and methanol permeability. The thermal and chemical stability of the membrane are also investigated. Moreover, the effects of plasticizers on the membrane are evaluated in terms of its morphology.

MATERIALS AND METHODS

Materials

Chitosan was synthesized in the previous study with a degree of deacetylation ⩾75% [7, 9]. All chemicals including Pluronic F127, mesitylene, potassium chloride, phosphotungstic acid, methanol, ethanol, glycerol, sodium hydroxide, sodium chloride, hydrogen peroxide, and iron (II) sulfate (FeSO$_4$) were obtained from Merck, Darmstadt, Germany. Aquadest and ultra-high purity nitrogen gas were obtained from a local company in Surabaya, Indonesia.

Preparation of m-PTA

The polyoxometalate-based filler was prepared through the hydrothermal method with 2 steps of calcination. Initially, copolymer blocks of Pluronic F127, mesitylene, KCl, and PTA were added to aquadest and stirred at room temperature for 4 h. The mixture was warmed at 35 °C for 24 h and followed by hydrothermal heating at 100 °C for 72 h. The residue was dried at 70 °C, followed by washing with ethanol repeatedly. The residue was calcined at a heating rate of 2 °C/min until 250 °C. The second calcination was conducted at 350 °C for 24 h with airflow [11]. The dried powder was further analyzed and denoted as m-PTA.

Fabrication of Cs/gly/m-PTA membranes

The Cs/gly/m-PTA membranes were fabricated using the solvent-evaporation method. Initially, 2 g of Cs powder was dissolved in 2% (v/v) acetic acid. Then, the Cs dope solution was gradually added to the gly and m-PTA fillers. The dope solution was cast on the acrylic plate and dried at room temperature. The dried membrane was washed using a 1 M NaOH solution to avoid the over-swelling of the membrane in water. Then, the membrane was neutralized with aquadest and dried at room temperature. The compositions of gly in the membranes are listed in Table 1.

Table 1 Compositions of the membranes.

Membrane	Cs (wt.%)	Gly (wt.%)	m-PTA (wt.%)	Acetic acid (wt.%)
Cs	2	–	–	98.00
Cs/m-PTA	2	–	0.20	97.80
Cs/gly-0.25/m-PTA	2	0.25	0.20	97.55
Cs/gly-0.50/m-PTA	2	0.50	0.20	97.30
Cs/gly-0.75/m-PTA	2	0.75	0.20	97.05
Cs/gly-1/m-PTA	2	1.00	0.20	96.80

Characterization methods

The functional groups of all materials were evaluated using the Fourier transform infrared (FTIR) 8400S (Shimadzu, Kyoto, Japan), and the pellet containing the sample and KBr powder was scanned at a range of 4000–400 cm^{-1}. The crystal phase of the membranes was also analyzed using X-ray diffraction (XRD) Xpert MPD (Malvern Panalytical, Worcestershire, UK) scanned from 0–60 °C using Cu Kα radiation. All samples were analyzed at 40 kV and 30 mA. The morphology of the membranes was characterized using a scanning electron microscope and energy dispersive X-ray (SEM-EDX) Zeiss Evo MA-10 (Carl Zeiss AG, Jena, Germany) with an accelerating voltage of 20 kV. The thermal stability of the membranes was evaluated by thermogravimetric analysis (TGA) Pyris 1 Analyzer (PerkinElmer Inc., Massachusetts, USA) with a heating rate of 5 °C/min from 25–500 °C. The N$_2$ adsorption-desorption analysis was only conducted to evaluate the pore size of the m-PTA. The m-PTA powder was degassed at 300 °C for 3 h to remove the absorbed gas by m-PTA, and the measurement was conducted in a vacuum environment. The data was collected using the Quantachrome NovaWin gas sorption instrument (Quantachrome Instruments, Florida, USA).

Membrane properties characterization

Proton conductivity

The proton conductivity of the membranes was evaluated using electrochemical impedance spectroscopy (EIS) Autolab PGSTAT204 (Metrohm AG, Herisau, Switzerland). The analysis was conducted at room temperature and was hydrated. The membranes were immersed in water for 24 h and placed between the 2 electrodes that were attached in a Teflon block. The analysis was scanned at the frequency range of 0.1 Hz to 1 MHz at the oscillating voltage of 10–100 mV. The measurement of proton conductivity is shown in Eq. (1).

$$\sigma = L/(R \times A) \qquad (1)$$

where σ is denoted as proton conductivity (S/cm), R as the resistance (Ω), and L and A as the thickness (cm) and surface area (cm^2) of the membrane, respectively.

Methanol permeability

The permeability measurement was conducted using 2 compartments containing distilled water (compartment A) and 2 M methanol solution (compartment B). The membrane was initially placed between those compartments before the solution was poured into the compartments and it was stirred constantly. The solution in compartment A was taken gradually every 30 min. The steps were repeatedly done until 360 min, and the permeability of the membranes was measured using Eq. (2).

$$P = (\Delta C_B/\Delta t) \times [(d \times V_a)/(A \times C_B)] \qquad (2)$$

where $\Delta C_B/\Delta t$ is denoted as the slope of methanol concentration in compartment B as a function of time (M/s), P is the membrane permeability (cm^2/s), A is the surface area (cm^2), d is the membrane thickness (cm), V_A is the water volume in compartment A (cm^3), and C_B is the methanol concentration in compartment B (M).

Membrane selectivity

The membrane selectivity was obtained from the ratio of proton conductivity and permeability of the membrane. The high selectivity is obtained due to the high proton conductivity and low methanol permeability. The high selectivity is favorable for DMFC application. The selectivity of the membrane is measured as written in Eq. (3).

$$S = \sigma/P \qquad (3)$$

where S is denoted as selectivity (S s/cm^3), σ as proton conductivity (S/cm), and P as the methanol permeability (cm^2/s).

Water and methanol uptake

The membranes were initially weighed and immersed in the distilled water and methanol in the separated glassware. The membranes were soaked for 24 h at room temperature. After immersion, the membranes were gently dried with tissue paper and weighed again denoted as wet membranes. The water (WU) and methanol uptake (MU) of the membranes were measured using Eq. (4).

$$\text{Uptake (\%)} = \left[(W_{\text{wet}} - W_{\text{dry}})/W_{\text{dry}}\right] \times 100\% \qquad (4)$$

where W_{dry} (g) and W_{wet} (g) are denoted as the weight of membranes before and after immersion in distilled water or methanol.

Ion exchange capacity (IEC)

The IEC of the membrane was evaluated by the titration method. The dried membrane was soaked in the 1 M NaCl solution for 24 h. Then, the membrane was removed, and the solution was titrated using 0.01 M NaOH with phenolphthalein as the indicator. The IEC was measured using Eq. (5).

$$\text{IEC (mmol/g)} = (V_{\text{NaOH}} \times M_{\text{NaOH}})/W_{\text{dry}} \qquad (5)$$

where V_{NaOH} is denoted as the titrated volume of NaOH (ml), M_{NaOH} is the molarity of NaOH (M), and W_{dry} is the weight of the dried membrane (g).

Oxidative stability (OS)

The chemical stability of the membrane was evaluated using a Fenton reagent containing 3% of H_2O_2 and 2 ppm of $FeSO_4$. The dried membrane was initially weighed and then soaked in the Fenton reagent for 1 h at 80 °C. The membrane was weighed again, and the weight loss of the membrane before and after immersion in the Fenton reagent was determined using Eq. (6).

$$OS\ (\%) = [(W_1 - W_2)/W_1] \times 100\% \qquad (6)$$

where W_1 (g) and W_2 (g) are the weight of the membrane before and after immersion in the Fenton reagent, respectively.

RESULTS AND DISCUSSION

The characteristics of m-PTA filler

The XRD spectra of PTA and m-PTA filler are shown in Fig. 1, which indicates the transformation of PTA to mesoporous form according to its crystal phases. The significant transformation of PTA to m-PTA is exhibited by the sharp peaks of the m-PTA diffractogram, which revealed an arranged structure of m-PTA due to the self-assembly of the PTA molecules and hydrothermal processes during the synthesis [11]. Furthermore, the typical peak of m-PTA filler is shown at the (222) plane at $2\theta = 27°$. The other peaks are also detected, including the planes of (110), (200), (220), (330), (510), and (611) [20]. Fig. 1c also confirms the presence of the mesoporous feature in m-PTA, as shown in low-angle XRD that only showed a sharp peak. The different patterns of pristine PTA and m-PTA are due to the self-assembly process and ion exchange at the beginning of the reaction between K^+ and H^+ that occurred in KCl and $H_3PW_{12}O_{40}$ [11].

The result of the isotherm method showed the pore diameter and surface area of the m-PTA filler. The pore diameter of m-PTA was achieved at 3.71 nm with a surface area of 9.621 m^2/g. The range of mesoporous pore diameter between 2–50 nm of the prepared m-PTA is included in the range of mesoporous material [21]. The large surface area of m-PTA also revealed the decline of the blockage process in the m-PTA pores by the tungsten molecule [11]. It is also denoted that the m-PTA filler is classified as the type-IV isotherm model according to its hysteresis loop indicating the differences in concentration of N_2 gas absorbed and N_2 gas desorbed at a steady pressure [20]. The type-IV isotherm can also indicate that the PTA transformed into its mesoporous structure. The isotherm model is shown in Fig. 2a.

The morphology of m-PTA indicates a clear spherical pattern with an average particle size of 730 nm that was created during the synthesis, and Pluronic F127 acts as the template of PTA [12]. The template was removed during the calcination at high temperature,

and the PTA molecules remained in a spherical structure [22]. Moreover, the pores of m-PTA were created as a result of the effective screening of PTA molecules by the surfactant [11]. The morphology of the m-PTA filler is shown in Fig. 2b and Fig. 2c.

The characteristics of Cs/gly/m-PTA membrane

The FTIR spectra of Cs/gly/m-PTA are shown in Fig. 3 which exhibit the bands of PTA and Cs. The bands of PTA are detected in 1026 cm^{-1} and 1376 cm^{-1} indicating the functional group of W=O and PO_4, respectively [23]. The Cs bands were also found in the wavenumber of 3354, 2872, 1644, and 1586 cm^{-1} denoted as −O−H, −C−H, and −C=O groups, respectively [7]. The −C−N group also appeared in the Cs bands at a wavenumber of 1022 cm^{-1}. However, the interaction of gly within the Cs and PTA resulted in a rising in the peak intensity of −OH and −C−H groups due to the hydroxyl and alkyl groups of gly incorporated into the membrane structure [4]. The broadening peaks of −O−H and −C−H in Cs indicate the functional groups only achieved from the Cs itself [24].

The diffractogram of the membranes is shown in Fig. 4 which reveals the significant differences between the Cs membrane, Cs/m-PTA, and Cs/gly/m-PTA membrane. The Cs membrane only shows 2 major peaks at $2\theta = 10°$ and $2\theta = 20°$, demonstrating the typical peaks of Cs [9]. Furthermore, the addition of m-PTA gives rise to new crystalline phases in the Cs membrane. The characteristic peak of m-PTA at $2\theta = 27°$ represents a (222) plane found in both Cs/m-PTA and Cs/gly/m-PTA membranes. However, the incorporation of gly in the Cs/m-PTA structure can improve the amorphous character of the membrane as well as the Cs itself, as shown in Fig. 4c [25]. The shifting of the m-PTA peaks in the Cs/gly/m-PTA membrane is due to the possible interaction of PTA and gly molecules incorporated into the Cs polymer backbone, which exhibited the changing of its crystalline features [23].

The morphology of the membranes is shown in Fig. 5 with the mapping elements of the membranes. It showed the Cs membrane only possessed N, O, and C elements. However, the Cs/m-PTA and Cs/gly/m-PTA have additional elements, including O, P, and W that are obtained from PTA molecules [11]. The addition of gly can avoid the agglomeration of the inorganic filler that is shown by the Cs/gly/m-PTA membrane. Its surface shows more homogeneity than the Cs/m-PTA membrane which clearly shows the agglomeration between PTA and Cs. Moreover, all membranes show a dense structure due to the fabrication method of the membranes. The solvent-evaporation method tends to create a non-porous membrane due to the slow phase inversion by airflow at ambient temperature [26].
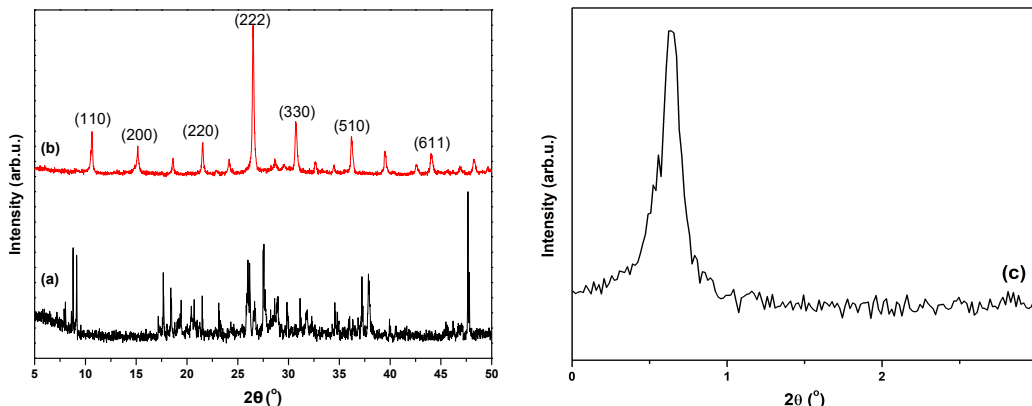
Fig. 1 XRD of PTA and m-PTA filler. Wide angle XRD of (a) pristine PTA, (b) m-PTA, and (c) low angle XRD of m-PTA.
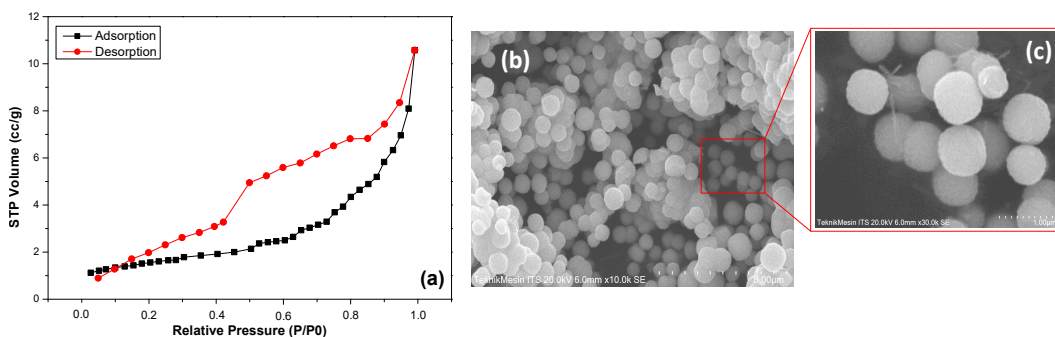

Fig. 2 Characteristics of m-PTA filler. (a) N_2 adsorption-desorption of m-PTA, (b) morphology of m-PTA at a magnification of 10,000×, and (c) 30,000×.
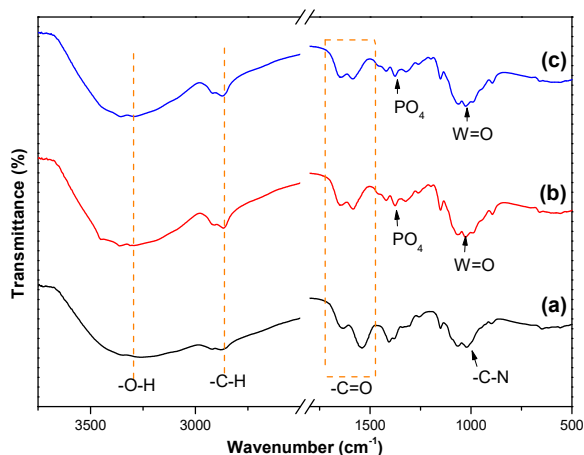

Fig. 3 FTIR spectra of composite membranes. (a) Cs membrane, (b) Cs/m-PTA, and (c) Cs/gly/m-PTA composite membrane.
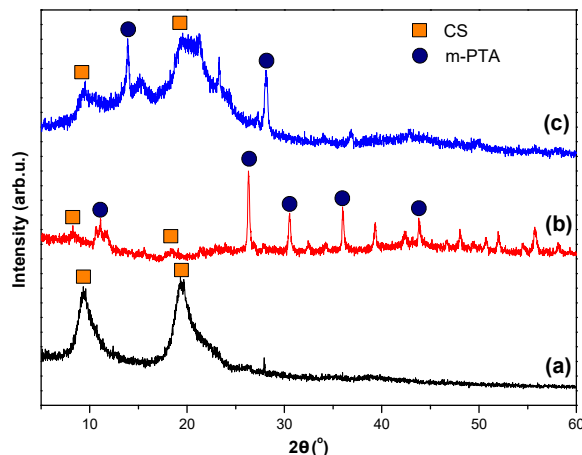
Fig. 4 XRD of composite membranes. (a) Cs membrane, (b) Cs/m-PTA, and (c) Cs/gly/m-PTA composite membrane.

The properties of Cs/gly/m-PTA membrane

The properties of the membranes were evaluated for their stability and uptake including thermal and chem-ical stability as well as water and methanol uptake. The thermal stability of the Cs/gly/m-PTA membrane is shown in Fig. 6a and Fig. 6b. The membrane shows an improvement in its stability, and the first degrada-tion indicates the membrane only lost its weight by
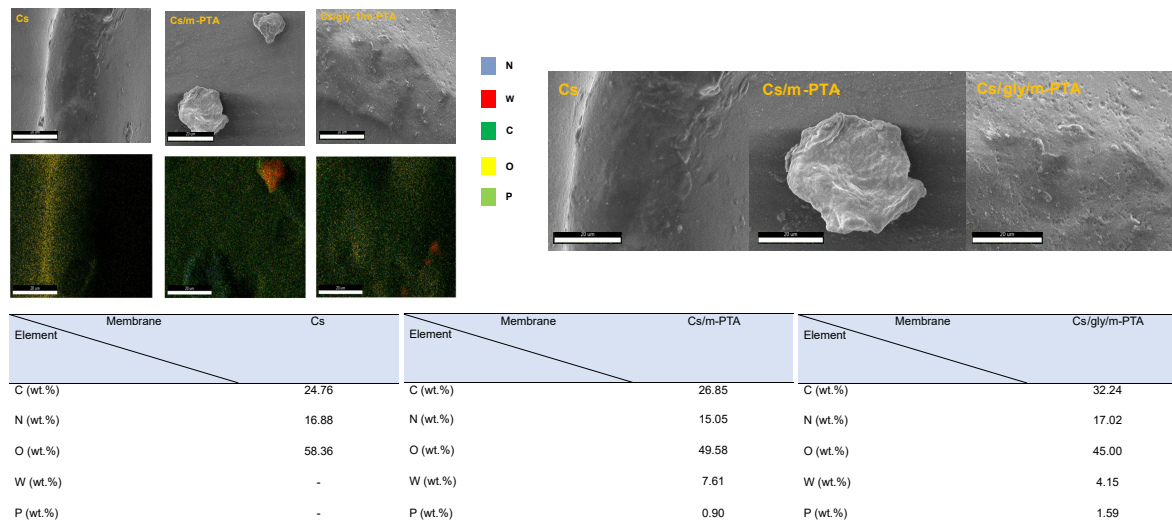
	Membrane	Cs
Element		
C (wt.%)		24.76
N (wt.%)		16.88
O (wt.%)		58.36
W (wt.%)		-
P (wt.%)		-

	Membrane	Cs/m-PTA
Element		
C (wt.%)		26.85
N (wt.%)		15.05
O (wt.%)		49.58
W (wt.%)		7.61
P (wt.%)		0.90

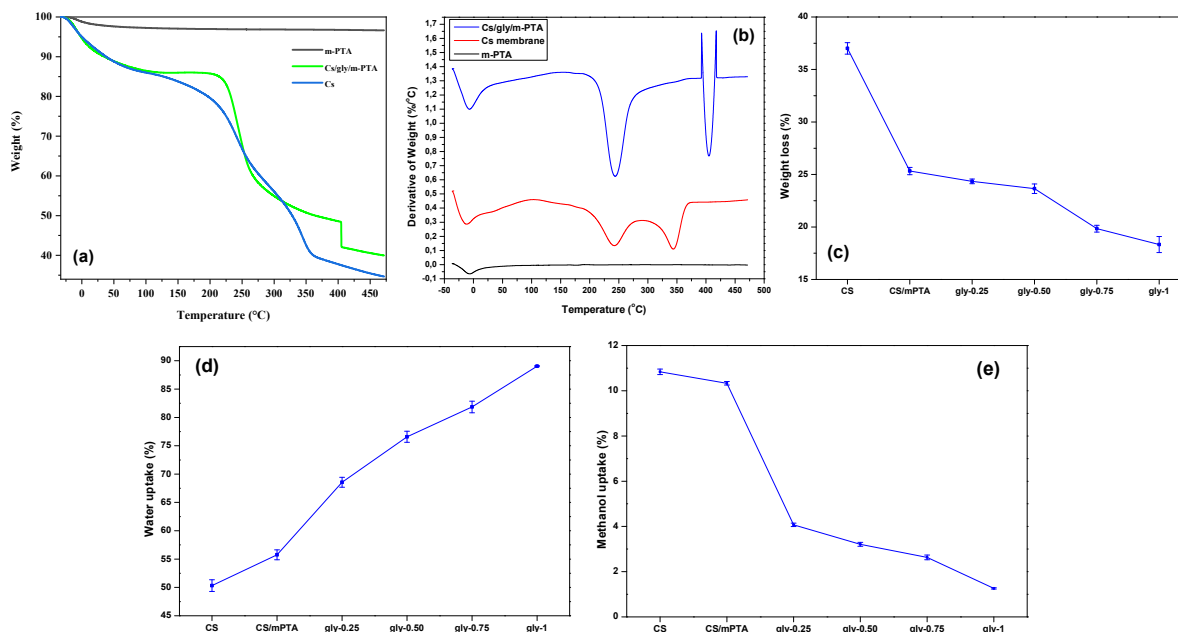|	Membrane	Cs/gly/m-PTA
Element		
C (wt.%)		32.24
N (wt.%)		17.02
O (wt.%)		45.00
W (wt.%)		4.15
P (wt.%)		1.59

Fig. 5 Morphology of the membranes by SEM-EDX.

Fig. 6 Properties of the membranes. (a) TGA profile, (b) DTG profile, (c) oxidative stability, (d) water uptake, and (e) methanol uptake of the membranes.

around 15 wt.% until 225 °C. As a comparison, the Cs membrane lost its weight by 20 wt.%. The first degradation of the Cs membrane is assigned to the loss of its water content and weakly bonded molecules [27]. This phenomenon can be affected by the addition of m-PTA filler. The m-PTA filler itself only has a weight loss and cannot lose its weight above 10 wt.% until 450 °C showing the thermal stability characteristic [22]. As mentioned in the previous study, the Keggin structure of PTA started to collapse at the higher temperature than 450 °C, resulting in the WO_3 and PO_x

molecules [11].

The oxidative stability of the membranes is shown in Fig. 6c which shows that the Cs/gly-1/m-PTA membrane has the lowest weight loss among the other membranes. Its weight loss for 1 h at 80 °C is 18.33±0.762% compared to the pristine Cs membrane the weight loss of which is 37.01±0.547%, followed by the Cs/m-PTA membrane at 24.33±0.346%. The reasons for the decreasing value of its weight are affected by the outstanding interaction between biopolymer, gly, and m-PTA filler. Many chemical interactions are

Table 2 Performances of the membranes.

Membrane	Methanol Permeability (cm^2/s)	IEC (mmol/g)	Proton Conductivity (mS/cm)	Selectivity (S s/cm^3)	Reference
Cs	1.003×10^{-5}	0.698 ± 0.105	2.40	2.39×10^2	This work
Cs/m-PTA	7.806×10^{-6}	0.788 ± 0.087	3.30	4.23×10^2	This work
Cs/gly-0.25/m-PTA	7.372×10^{-6}	1.091 ± 0.122	3.61	4.89×10^2	This work
Cs/gly-0.50/m-PTA	5.984×10^{-6}	1.225 ± 0.132	4.34	7.25×10^2	This work
Cs/gly-0.75/m-PTA	2.021×10^{-6}	1.606 ± 0.091	4.83	2.39×10^3	This work
Cs/gly-1/m-PTA	1.982×10^{-6}	2.949 ± 0.022	5.13	2.58×10^3	This work
Pristine Cs	1.050×10^{-4}	0.230 ± 0.067	2.86	–	[9, 23]
Cellulose/PTA	3.540×10^{-7}	0.359	0.11	2.99×10^2	[34]

involved in creating a durable membrane that is chemically stable [28]. Furthermore, the polyoxometalate-based filler can protect the Cs biopolymer from further oxidation by forming a highly stable molecular network as the gly can as a plasticizer that develops cross-linked polymer chains [27].

The water and methanol uptake of the membranes are shown in Fig. 6d and Fig. 6e, respectively. The water uptake of the membranes was improved with the addition of gly to the membranes. The highest water uptake was obtained by the Cs/gly-1/m-PTA membrane at 89.05±0.092%, and the lowest was the Cs membrane at 50.32±1.033%. The improvement of its water uptake was influenced by gly in that more hydroxyl groups were attached to the membrane structure giving more hydrophilic sites in the membrane [29]. In addition, the methanol uptake of the membranes tends to decrease with the addition of m-PTA and gly. According to the previous study, the polyoxometalate-based filler and enhanced interaction between gly and m-PTA in the membrane can develop long diffusion pathways for the methanol to avoid the loss of fuel in the membrane and maintain fuel efficiency [30]. Low methanol uptake and high water uptake are favorable for the PEM in DMFC [7]. In this research, the lowest methanol uptake was Cs/gly-1/m-PTA at 1.26±0.031% with Cs and Cs/m-PTA at 10.84±0.121% and 10.33±0.079%, respectively.

The performances of Cs/gly/m-PTA membrane

All performances are listed in Table 2 including proton conductivity, methanol permeability, IEC, and selectivity. The methanol permeability of the membranes shows a diminishing permeability trend with the addition of gly and m-PTA. The homogeneously dispersed filler creates a methanol barrier network with long diffusion pathways in the membrane [6]. Since the diffusion method was applied for PEM, the longer diffusion pathway is preferable for PEM and can be achieved by cross-linking between polymer, gly, and filler [31]. The result of permeability is in agreement with the methanol uptake value. With the addition of

gly and m-PTA, the methanol permeability and uptake dropped to a lower value. The permeability of the Cs/gly-1/m-PTA is 1.986×10^{-6} cm^2/s as compared to the Nafion 115 which is 5.65×10^{-5} cm^2/s [20].

The trend in IEC denotes that the enrichment of hydrophilic groups increases the IEC of the membranes. The highest IEC was also achieved by Cs/gly-1/m-PTA which can be affected by the extra hydrophilic groups obtained from gly. The improvement of IEC is very important to improve the proton conductivity of the membrane as well [32]. The IECs of Cs and Cs/gly-1/m-PTA membranes were 0.689±0.105 and 2.949±0.022 mmol/g, respectively. It denoted more than twice the increment from Cs. At the same operating conditions, Nafion only achieves its IEC at 0.860 mmol/g [33].

The proton conductivity of the Cs/gly-1/m-PTA membrane shows improvement compared to the Cs membrane. The improvement could be due to the high surface area of m-PTA which increases the charge per unit area facilitating the proton transfer of the membranes [11]. Moreover, the excess of hydrophilic groups supported by gly gives the new proton channel for H$^+$ to transfer through the membrane easily [4]. However, the proton conductivity of Cs/gly-1/m-PTA is still lower than that of Nafion 115 at room temperature (28 mS/cm) [33]. The selectivity of the membrane was also affected by methanol permeability and proton conductivity. The high conductivity and low permeability generate high selectivity for the membrane [20]. In this research, the selectivity of Cs/gly-1/m-PTA is higher than that of the Cs membrane at 2.58×10^3 S s/cm^3, and with the addition of gly, the selectivity also increased. The possible interaction, fuel permeation, and proton conductivity mechanism are shown in Fig. 7.

CONCLUSION

In this research, the composite membranes of Cs/gly/m-PTA were successfully fabricated using the solvent-evaporation method and achieved an improvement in fuel cell performances. The Cs/gly-1/m-PTA membrane is the membrane that achieved the
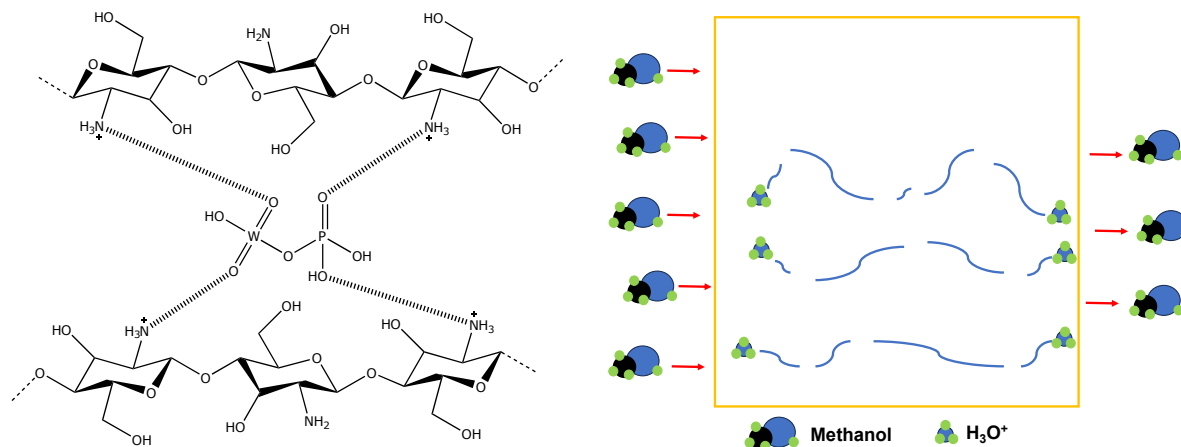
Fig. 7 Possible interaction and mechanism of the conductivity and fuel permeation.

lowest methanol uptake and permeability. The highest proton conductivity of the membrane is 5.13 mS/cm, which is better than the unmodified Cs membrane. Furthermore, the addition of m-PTA and gly can improve the thermal and chemical stability of the Cs membrane. Both water uptake and the IEC of the membrane increase with the addition of gly. In this research, the high selectivity of Cs/gly-1/m-PTA was also achieved, along with low permeability and a high proton conductivity value.

REFERENCES

1. Mohamad Nor NA, Nakao H, Jaafar J, Kim JD (2020) Crosslinked carbon nanodots with highly sulfonated polyphenylsulfone as proton exchange membrane for fuel cell applications. *Int J Hydrogen Energy* **45**, 9979–9988.
2. Wang W, Shan B, Zhu L, Xie C, Liu C, Cui F (2018) Anatase titania coated CNTs and sodium lignin sulfonate doped chitosan proton exchange membrane for DMFC application. *Carbohydr Polym* **187**, 35–42.
3. Muhmed SA, Jaafar J, Daud SS, Hanifah MFR, Purwanto M, Othman MHD, Rahman MA, Ismail AF (2021) Improvement in properties of nanocrystalline cellulose/poly(vinylidene fluoride) nanocomposite membrane for direct methanol fuel cell application. *J Environ Chem Eng* **9**, 105577.
4. Shaari N, Kamarudin SK (2018) Performance of crosslinked sodium alginate/sulfonated graphene oxide as polymer electrolyte membrane in DMFC application: RSM optimization approach. *Int J Hydrogen Energy* **43**, 22986–23003.
5. Ranjani M, Pannipara M, Al-Sehemi AG, Vignesh A, Kumar GG (2019) Chitosan/sulfonated graphene oxide/silica nanocomposite membranes for direct methanol fuel cells. *Solid State Ionics* **338**, 153–160.
6. Purwanto M, Atmaja L, Mohamed MA, Salleh MT, Jaafar J, Ismail AF, Santoso M, Widiastuti N (2016) Biopolymer-based electrolyte membranes from chitosan incorporated with montmorillonite-crosslinked GPTMS for direct methanol fuel cells. *RSC Adv* **6**, 2314–2322.
7. Priyangga A, Mumtazah Z, Junoh H, Jaafar J, Atmaja L (2021) Morphology and topography studies of composite membranes developed from chitosan/phthaloyl chitosan consisting multi-walled carbon nanotube/montmorillonite as filler. *J Membr Sci Res* **7**, 295–304.
8. Liu G, Tsen WC, Jang SC, Hu F, Zhong F, Liu H, Wang G, Wen S, et al (2019) Mechanically robust and highly methanol-resistant sulfonated poly(ether ether ketone)/poly(vinylidene fluoride) nanofiber composite membranes for direct methanol fuel cells. *J Memb Sci* **591**, 117321.
9. Nurakhirawati N, Priyangga A, Santoso M (2022) Physicochemical studies of chitosan blended sulfonated poly ether-ether ketone and graphene oxide as filler for direct methanol fuel cell. *Defect Diffus Forum* **416**, 173–181.
10. Pasini Cabello SD, Ochoa NA, Takara EA, Mollá S, Compañ V (2017) Influence of pectin as a green polymer electrolyte on the transport properties of chitosan-pectin membranes. *Carbohydr Polym* **157**, 1759–1768.
11. Ilbeygi H, Kim IY, Kim MG, Cha W, Kumar PSM, Park DH, Vinu A (2019) Highly crystalline mesoporous phosphotungstic acid: a high-performance electrode material for energy-storage applications. *Angew Chemie Int Ed* **58**, 10849–10854.
12. Mohanapriya S, Raj V (2018) Cesium-substituted mesoporous phosphotungstic acid embedded chitosan hybrid polymer membrane for direct methanol fuel cells. *Ionics (Kiel)* **24**, 2729–2743.
13. Liu H, Gong C, Wang J, Liu X, Liu H, Cheng F, Wang G, Zheng G, et al (2016) Chitosan/silica coated carbon nanotubes composite proton exchange membranes for fuel cell applications. *Carbohydr Polym* **136**, 1379–1385.
14. Terbish N, Lee CH, Popuri SR, Nalluri LP (2020) An

investigation into polymer blending, plasticization and cross-linking effect on the performance of chitosan-based composite proton exchange membranes for microbial fuel cell applications. *J Polym Res* **27**, 280.

15. Hadi JM, Aziz SB, Saeed SR, Brza MA, Abdulwahid RT, Hamsan MH, Abdullah RM, Kadir MFZ, et al (2020) Investigation of ion transport parameters and electrochemical performance of plasticized biocompatible chitosan-based proton conducting polymer composite electrolytes. *Membranes (Basel)* **10**, 363.

16. Shaari N, Kamarudin SK (2019) Recent advances in additive-enhanced polymer electrolyte membrane properties in fuel cell applications: an overview. *Int J Energy Res* **43**, 2756–2794.

17. da Trindade LG, Borba KMN, Zanchet L, Lima DW, Trench AB, Rey F, Diaz U, Longo E, et al (2019) SPEEK-based proton exchange membranes modified with MOF-encapsulated ionic liquid. *Mater Chem Phys* **236**, 121792.

18. Gnana Kumar G, Manthiram A (2017) Sulfonated polyether ether ketone/strontium zirconite@TiO$_2$ nanocomposite membranes for direct methanol fuel cells. *J Mater Chem A* **5**, 20497–20504.

19. Ranjani M, Al-Sehemi AG, Pannipara M, Aziz MA, Phang SM, Ng FL, kumar GG (2020) SnO$_2$ nanocubes/bentonite modified SPEEK nanocomposite composite membrane for high performance and durable direct methanol fuel cells. *Solid State Ionics* **353**, 115318.

20. Priyangga A, Atmaja L, Santoso M, Jaafar J, Ilbeygi H (2022) Utilization of mesoporous phosphotungstic acid in nanocellulose membranes for direct methanol fuel cells. *RSC Adv* **12**, 14411–14421.

21. Miri S, Raghuwanshi VS, Andrews PC, Batchelor W (2021) Composites of mesoporous silica precipitated on nanofibrillated cellulose and microfibrillated cellulose: effect of fibre diameter and reaction conditions on particle size and mesopore diameter. *Microporous Mesoporous Mater* **311**, 110701.

22. Mohamed MH, Ilbeygi H, Jaafar J, Aziz M, Othman MHD, Rahman MA (2022) Influence of mesoporous phosphotungstic acid on the physicochemical properties and performance of sulfonated poly ether ether ketone in proton exchange membrane fuel cell. *Int J Hydrogen Energy* **47**, 10736–10746.

23. Kim AR, Park CJ, Vinothkannan M, Yoo DJ (2018) Sulfonated poly ether sulfone/heteropoly acid composite membranes as electrolytes for the improved power generation of proton exchange membrane fuel cells. *Compos Part B Eng* **155**, 272–281.

24. Atmaja L, Purwanto M, Salleh MT, Mohamed MA, Jaafar J, Ismail AF, Santoso M, Widiastuti N (2019) GPTMS-montmorillonite-filled biopolymer chitosan membrane with improved compatibility, physicochemical, and thermal stability properties. *Malaysian J Fundam Appl Sci* **15**, 492–497.

25. Gil-Castell O, Teruel-Juanes R, Arenga F, Salaberria AM, Baschetti MG, Labidi J, Badia JD, Ribes-Greus A (2019) Crosslinked chitosan/poly(vinyl alcohol)-based polyelectrolytes for proton exchange membranes. *React Funct Polym* **142**, 213–222.

26. Junoh H, Jaafar J, Nik Abdul NAH, Ismail AF, Othman MHD, Rahman MA, Aziz F, Yusof N, et al (2021) Porous polyether sulfone for direct methanol fuel cell applications: structural analysis. *Int J Energy Res* **45**, 2277–2291.

27. Anu Karthi AKS, Cindrella L (2019) Self-humidifying novel chitosan-geopolymer hybrid membrane for fuel cell applications. *Carbohydr Polym* **223**, 115073.

28. Gaur SS, Dhar P, Sonowal A, Sharma A, Kumar A, Katiyar V (2017) Thermo-mechanically stable sustainable polymer based solid electrolyte membranes for direct methanol fuel cell applications. *J Memb Sci* **526**, 348–354.

29. Vijayakumar V, Khastgir D (2018) Hybrid composite membranes of chitosan/sulfonated polyaniline/silica as polymer electrolyte membrane for fuel cells. *Carbohydr Polym* **179**, 152–163.

30. Hosseinpour M, Sahoo M, Perez-Page M, Baylis SR, Patel F, Holmes SM (2019) Improving the performance of direct methanol fuel cells by implementing multilayer membranes blended with cellulose nanocrystals. *Int J Hydrogen Energy* **44**, 30409–30419.

31. Sanchez-Salvador JL, Balea A, Monte MC, Negro C, Blanco A (2021) Chitosan grafted/cross-linked with biodegradable polymers: a review. *Int J Biol Macromol* **178**, 325–343.

32. Rath R, Kumar P, Unnikrishnan L, Mohanty S, Nayak SK (2021) Functionalized poly(vinylidene fluoride) for selective proton-conducting membranes. *Mater Chem Phys* **260**, 124148.

33. Wang J (2015) Barriers of scaling-up fuel cells: Cost, durability and reliability. *Energy* **80**, 509–521.

34. Bagus Pambudi A, Priyangga A, Hartanto D, Atmaja L (2020) Fabrication and characterization of modified microcrystalline cellulose membrane as proton exchange membrane for direct methanol fuel cell. *Mater Today Proc* **46**, 1855–1859.